Periodico di Mineralogia (2011), 80, 1 (Special Issue), 89-104 DOI: 10.2451/2011PM0007

PERIODICO di MINERALOGIA
established in 1930

An International Journal of
MINERALOGY, CRYSTALLOGRAPHY, GEOCHEMISTRY,
ORE DEPOSITS, PETROLOGY, VOLCANOLOGY
and applied topics on *Environment*, *Archeometry* and *Cultural Heritage*

Special Issue in memory of Sergio Lucchesi

Growth Marks of titanian-andradite crystals from Colli Albani (Italy)

Giovanna Agrosi*, Eugenio Scandale and Gioacchino Tempesta

Dipartimento Geomineralogico - Università degli Studi di Bari "Aldo Moro", Italy
*Corresponding author: *g.agrosi@geomin.uniba.it*

Abstract

Growth defects and chemical zonings of Ti-rich andradite (melanite) crystals from Colli Albani were studied using X-ray Diffraction Topography and Electron Probe Microanalysis in order to determine the distinctive features, "growth marks", characterising minerals grown directly from high temperature solution in an open system (volcanic chamber). The samples, cut in (110) and (001) slices, showed a number of primary and, above all, multiphasic melt inclusions, as well as, an unusual colour zoning consisting of a darker colour in the {211} growth sectors with the respect to the {110} sectors. The analysis of X-ray topographic contrasts of growth defects as growth bands, sector boundaries and bundles of dislocations developed parallel to the growth directions has enabled the reconstruction of the morphological evolution vs. time of the samples. The results also suggest that from their onset the crystals were faceted with {211}and predominant {110} faces. Moreover, the topographic images indicated that most of the examined dislocations were nucleated from inclusions. By using the extinction criterion, it was possible to determine that these defects are characterised by a strong edge component. The faceted morphology of garnets found in this paper and the fact that edge dislocations were only characterised suggest a layer spreading growth mechanism by two-dimensional nucleation. The reconstruction of morphology was also particularly useful in distinguishing two different types of chemical zoning: concentric and sector zoning. The results of chemical analyses confirmed that the optically observed colour zoning coincided with sector zoning because of a small but meaningful enrichment of TiO_2 and a decrease of Al_2O_3 in correspondence with {211} growth sectors. Instead, concentration variations, chiefly of TiO_2 and SiO_2, were recorded crossing successive growth stages. This event appeared to be associated with the physio-chemical evolution of the growth environment and was defined as concentric zoning. Comparing the results found in our study with those of previous studies on garnets from hydrothermal and metasomatic environments, the meaning of the growth marks in the Ti-rich andraditic garnets from Colli Albani could be assigned to primary multiphase melt inclusions, concentric and sector zoning, sector boundaries, growth bands and edge dislocations since these defects characterise and distinguish our samples from those grown in different genetic environments.

Key words: X-ray Topography; Ti-rich andradite; structural defects; concentric zoning; sector zoning.

Introduction

The study of relationships among structural defects, chemical zoning, morphology and crystal growth in minerals plays a basic role in the minero-petrogenetic field. In fact, growth defects and chemical zoning can represent a record of growth conditions and thus provide information about the evolution of a growth environment. Previous studies carried out to compare growth defects in minerals grown in the same conditions have shown that these minerals will have similar types of defects. These defects have been called growth marks since they represent distinctive defects that can help to identify whether minerals have grown under the same conditions or different ones, even if similar (Scandale et al., 1990). The "growth marks" concept has primarily been used in studies on natural crystals such as hydrothermal quartz (Scandale et al., 1983; Scandale e Stasi, 1985; Agrosì et al., 1992) and pegmatitic beryls (Scandale et al., 1990; Graziani et al., 1990) from different provenances. Recently, growth marks have also been employed in the study of tourmaline crystals from pegmatite pockets on Elba Island (Italy). These crystals exhibit a Mn-rich (greenish) core grown under pegmatitic conditions, and a Mn-free (colourless) elbaitic overgrowth grown under the hydrothermal stage of pegmatite crystallization (Bosi et al., 2005; Agrosì et al., 2006).

From all of the aforementioned studies, a common conclusion can be drawn: crystallization under pegmatitic and hydrothermal conditions produces different growth defects. Really, crystals which are grown under hydrothermal conditions show screw dislocations whereas minerals grown under pegmatitic conditions are screw-dislocation free. However, growth marks that give information about the growth mechanisms operating in orthomagmatic conditions have not yet been studied. With this in mind, Ti-rich andradite crystals from pyroclastic deposits of Colli Albani (Italy) have been investigated to try to determine the growth marks of minerals grown directly from high temperature solution in an open system (volcanic chamber). These minerals show a complex chemical zoning that consists of the superposition of sector and concentric zoning (Agrosì et al., 2001; Agrosì et al., 2002). In addition, their morphological perfection contrasts strikingly with an anomalous "anisotropy" found inside. Structural defects were studied by means of X-ray Diffraction Topography (XRDT) both with monochromatic radiation using a conventional source (Lang's camera) and with white beam radiation using a synchrotron source (SWBXT). Chemical zonings were investigated by Electron Microprobe Analysis (EPMA) and were then related to the structural defects.

Materials and Methods

The Ti-rich andradites discussed in this study came from pyroclastic deposits at Colli Albani, a Middle-Late Pleistocene volcanic complex belonging to a Roman Perpotassic Province (Lazio, Italy) (Fornaseri, 1963). These crystals are of centimetric size. They appear highly fractured and show a combination of well-developed $d\{110\}$ and $n\{211\}$ forms, with the former more developed than the latter (Figure 1a). The samples chosen for this study were cut parallel to the (110) plane and parallel to the (001) plane after having been enclosed in epoxy resin in order to prevent breakage. Structural defects were studied by means of X-ray Diffraction Topography (XRDT), an imaging technique based on Bragg diffraction, sensitive to the strain associated with distortions and extended crystalline defects in single crystals.

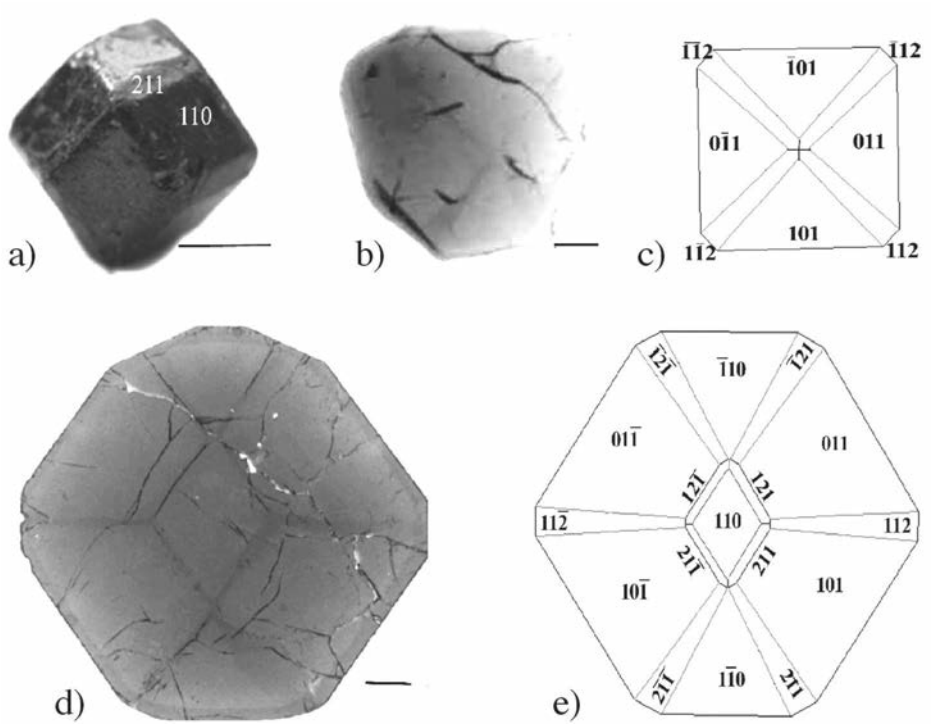

Figure 1. Ti-rich andradite from Colli Albani. a) a typical morphology of samples (bar scale = 5mm); b) colour zoning of {211} growth sectors in a (110) slice labelled M5 (bar scale = 1mm); c) schematic drawing corresponding to a theoretical (110) section; d) colour zoning of {211} growth sectors in a (001) slice labelled GRT (bar scale = 1mm); e) schematic drawing corresponding to a theoretical (001) section.

The XRDTs were taken in transmission geometry (Lang, 1959) using both synchrotron white beam (SWBXT) and conventional MoKα_1 radiation (XRDT). The XRDTs were carried out using a Rigaku camera and were performed under $\mu t \sim 1$ conditions (μ: linear absorption coefficient; t: crystal thickness) and recorded onto Ilford L4 photographic plates. In order to satisfy the $\mu t \sim 1$ condition, the obtained slices were thinned to a thickness of about 0.3 mm and then were mechanically polished on both sides.

SWBXTs were performed at the ID 19 beamline of the European Synchrotron Radiation Facility (Grenoble, France) and were recorded as Laue patterns on Kodak Industrex SR films with exposure times between 0.1-1 s and a crystal-film distance between 10-15 cm. The spatial resolution was about 5 μ. The LauePt program was used to index the Laue patterns (Huang, 2003).

Microanalyses were performed by means of a Cameca SX-50 Electron Microprobe at the Centro studio per il Quaternario e l'Evoluzione Ambientale del CNR Rome, with a ZAF 4/FLS data reduction system. Work conditions were as follows: accelerating potential of 15 KV; specimen beam current of 15 nA; counting time of 100 s; and beam diameter of 1 μm. The analyses were carried out by means of 5 WDS spectrometers for Ti, Al, Mg, Na, and K while EDS LINK spectrometers were used for Si, Ca,

Fe, Mn, P and Zr. The following standards were employed: jadeite (Na and Al); periclase (Mg); wollastonite (Si and Ca); apatite (P); rutile (Ti); orthoclase (K); pure Mn, magnetite (Fe) and zircon (Zr). A conversion from X-ray counts to oxide weight percentages (wt%) was carried out with the ZAF 4/FLS data reduction system.

The oxide totals in the accepted analyses always remained within 97-100 wt.%. Precision of major elements (Si, Al, Fe, Ti, and Ca) was within 1% of the actual amounts present, whereas that of minor elements (Mg, Mn, Zr, Na, K and P) was within about 10%. The compositional variations were measured by means of beam scanning, automatically stepping the microprobe beam at 50 and 100 μm steps. Spot analyses were also carried out on the solid inclusions which outcrop on the surface of the slices.

Results

Optical observations

Among all the samples investigated, four representative slices have been chosen to describe the results obtained in this paper: one (110) slice labelled MG and two (001) slices labelled M3 and M4 were used for the topographic investigations; and one (110) slice, labelled GRT, was used for the microanalytical analyses.

The slices present the typical brownish colour of Ti-rich andradite but with an unusual colour zoning. In the thin sections, the {211} growth sector projections appear slightly darker than the {110} projections (Figures 1b and 1c). Moreover, optical observations reveal the occurrence of some solid inclusions and a number of fluid inclusions. Transmitted light observations and EMPA indicate that the main solid inclusions consist of apatite and kalsilite. Conversely, the fluid inclusions observed on all the samples can be considered melt inclusions because they consist of silicate glass or its devitrified equivalent plus a shrinkage/vapour bubble and/or trapped mineral phases or daughter crystals. These inclusions were found to be chiefly multiphase and on rare occasion monophase. Their density and their orientation vary in the different slices: isolated and randomly oriented melt inclusions can be observed in the MG, GRT and M3 slices, whereas in the M4 sample a higher density of melt inclusions can be seen (Figure 2a). In this slice, most of melt inclusions are rod like radial inclusions elongated perpendicularly to the growing faces. Such inclusions can be classified as primary in origin since they are situated either isolated and randomly oriented or along the growth surfaces of the host crystal (Figure 2b). The length of the tubular primary inclusions is about 40 μm (Figure 2c).

Finally, two kinds of fractures can be seen in all the samples: sub-conchoidal fractures F (MG, GRT, M3 and M4) and rectilinear fractures (M3 and M4). The latter was observed only on slices parallel to (001) and corresponds to traces of {110} cleavage planes.

X-ray Topography

The analysis of structural defects was performed using both SWBXT and XRDT. The former yielded the highest achievable number of topographs. Indeed, SWBXT is a powerful technique that consists of projection topography in transmission Laue geometry using a polychromatic (white) beam. Each slice was placed into the beam without the need for exact adjustments. Many lattice planes met the reflection condition and formed a Laue pattern, hence, several topographs could be simultaneously recorded on one film exposure (Figure 3). Nevertheless, whenever it was necessary to improve contrast resolution to eliminate the effects caused by the polychromatic nature of SWBXTs (i.e. the superposition of the different harmonic components on the same topographic Laue spot), XRDTs with monochromatic radiation ($MoK\alpha_1$) and conventional source were also

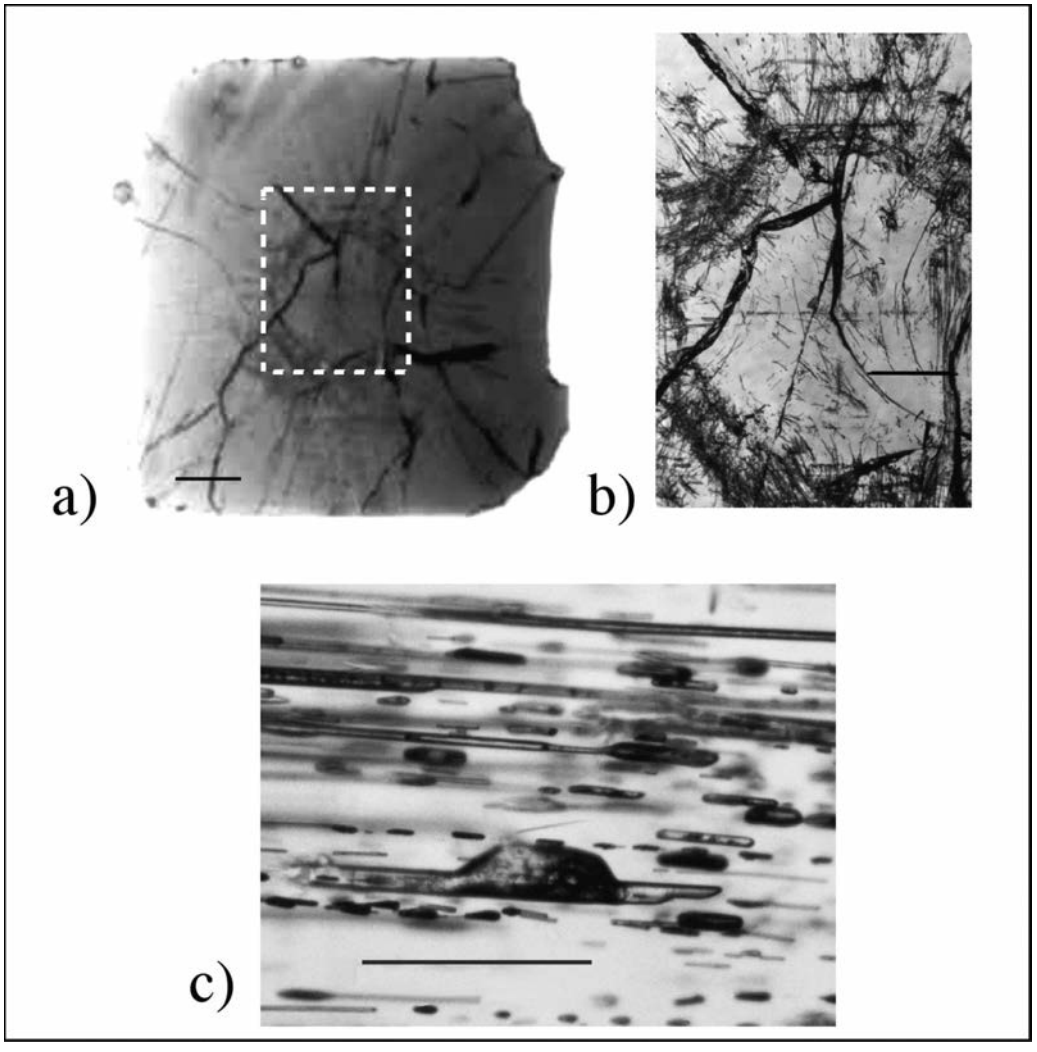

Figure 2. a) Micrograph of the (001) slice labelled M4 (bar scale = 1 mm); b) enlarged detail of core (bar scale = 500 μm). Note a kalsilite inclusion and melt inclusions randomly oriented and adsorbed along sector and growth stage boundaries; c) enlarged detail of melt inclusions running along the growth direction (bar scale = 150 μm). Note the crystallisation of daughter-mineral phases within the inclusions.

performed. The main defects observed on the topographs obtained were growth bands G, sector boundaries SB, dislocations D and fractures F (Figures 4, 5, 6 and 7).

The occurrence of several fractures caused different diffraction behaviour in the crystalline portions when the SWB or monochromatic radiation from conventional source bathed the slices. It can be observed that the fractures F bound areas misoriented up to a few degrees so that in

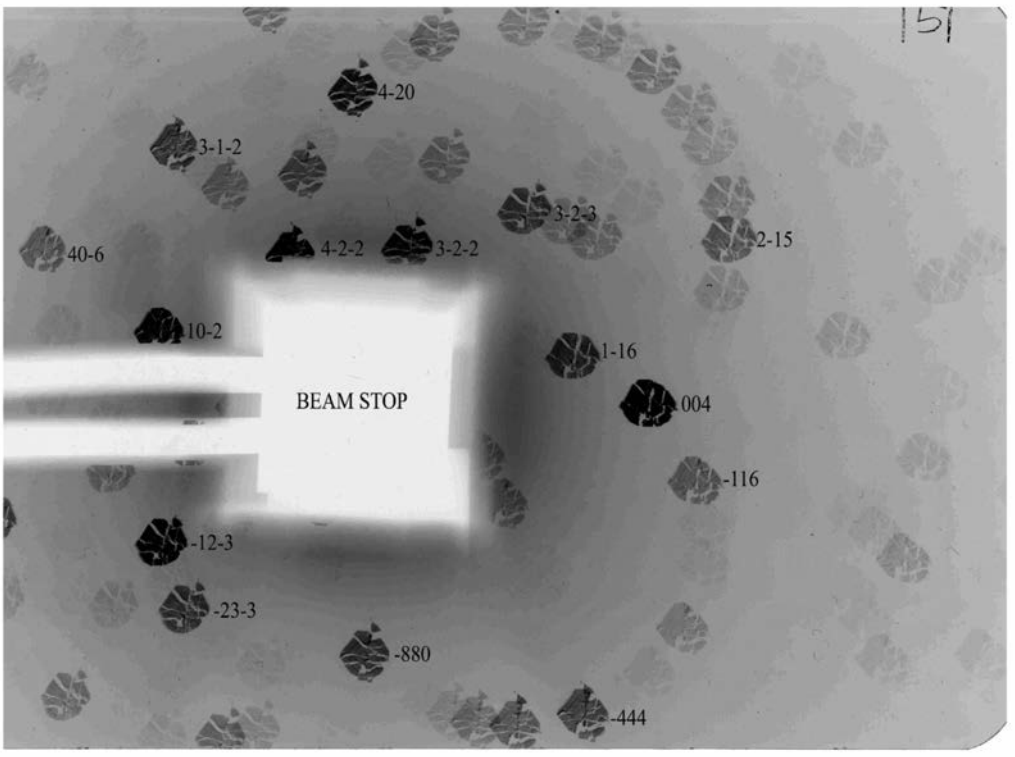

Figure 3. SWBXT: Laue pattern of the (110) MG slice.

the SWBXTs these areas are simultaneously in contrast even if the disorientation among them turn into a displacement of the corresponding images (Figures 4a, c; 6a, b; 7a, b). Instead, in the XRDTs, only some of the misoriented areas are in contrast for a given diffraction condition, whereas the remaining areas are out of reflection conditions (Figures 4b, 5b, 6c, d, e, 7c, d).

The growth bands G are mainly observed in the MG and M3 slices where the defect density is quite low (Figures 4, 5 and 6). In the MG slice, growth band contrasts G observed in the {110} growth sectors trace a sequence of four growth stages (Figure 4b). In particular, in growth sector (the origin at $\bar{1}10$), growth bands G observed with $\mathbf{g} = \bar{8}80$ (Figure 5b) are out of contrast with diffraction vector $\mathbf{g}=004$ (Figure 5a). Consequently, it could be concluded that, in this specific case, the strains responsible for the contrasts were due to deformations with displacement vector **u** normal to the growing faces. The extinction condition $|\mathbf{g} \cdot \mathbf{b}| = 0$ is then actually satisfied, where **b** is the Burgers vector (Azaroff, 1974).

The SB topographic contrasts outline the boundaries between the contiguous rombohedral *d* and trapezohedral *n* growth sectors (Figures 4, 5, 6 and 7) and allow their relative developments to be reconstructed. It can be noted that the *d*{110} growth sectors are more developed than the *n*{211} growth sectors and thus they must have grown more slowly. Moreover, the SB contrasts are rounded and denote an irregular shape of the growth sectors when compared with

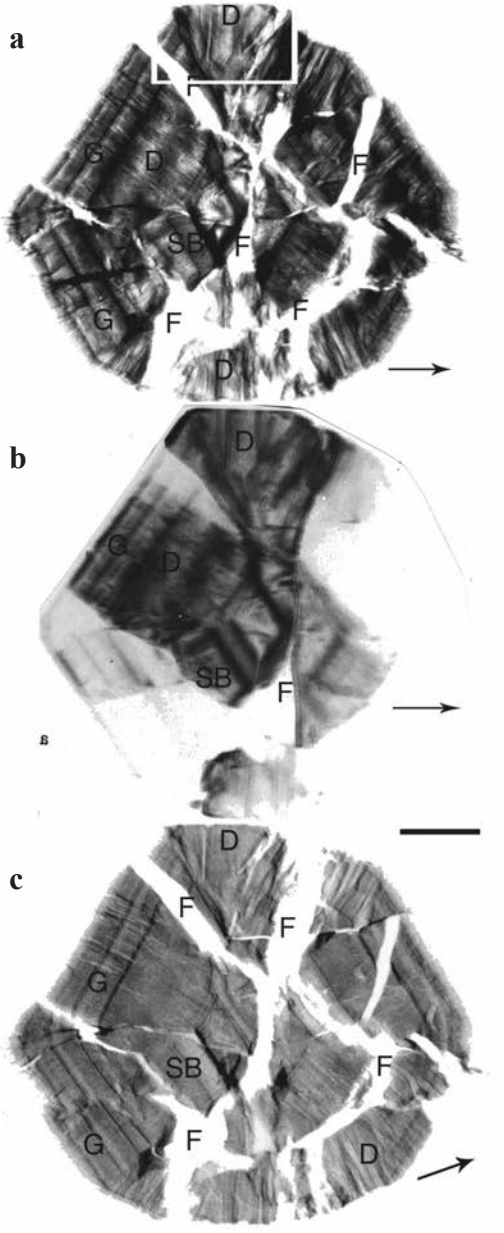

Figure 4. X-ray Topograps of the (110) MG slice (bar scale = 1mm). The arrows show the projection of diffraction vectors **g**. D: dislocations; SB: sector boundary; G growth band; F: fracture. a) SWBXT **g** = 004; b) XRDT **g** = 004; c) SWBXT **g** = $1\bar{1}6$.

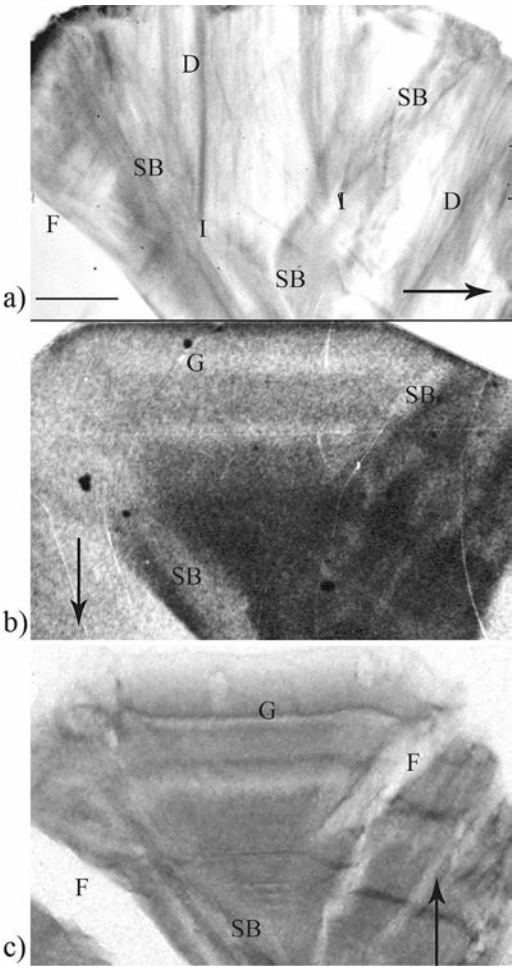

Figure 5. MG slice. Enlarged details of ($1\bar{1}0$) growth sector of X-ray Topograps (bar scale = 500 μm). The arrows show the projection of diffraction vectors g. G: growth bands; SB: sector boundaries; D: dislocations; F: fractures. I: solid inclusions. a) XRDT. Enlarged details of ($1\bar{1}0$) growth sector of topograp shown in Figure 4b. **g** = 004. Note the D nucleated from the I absorbed at the SB. b) XRDT. **g** = $\bar{8}80$. c) SWBXT. **g** = $\bar{3}20$. Note the extinction of D in the last two images.

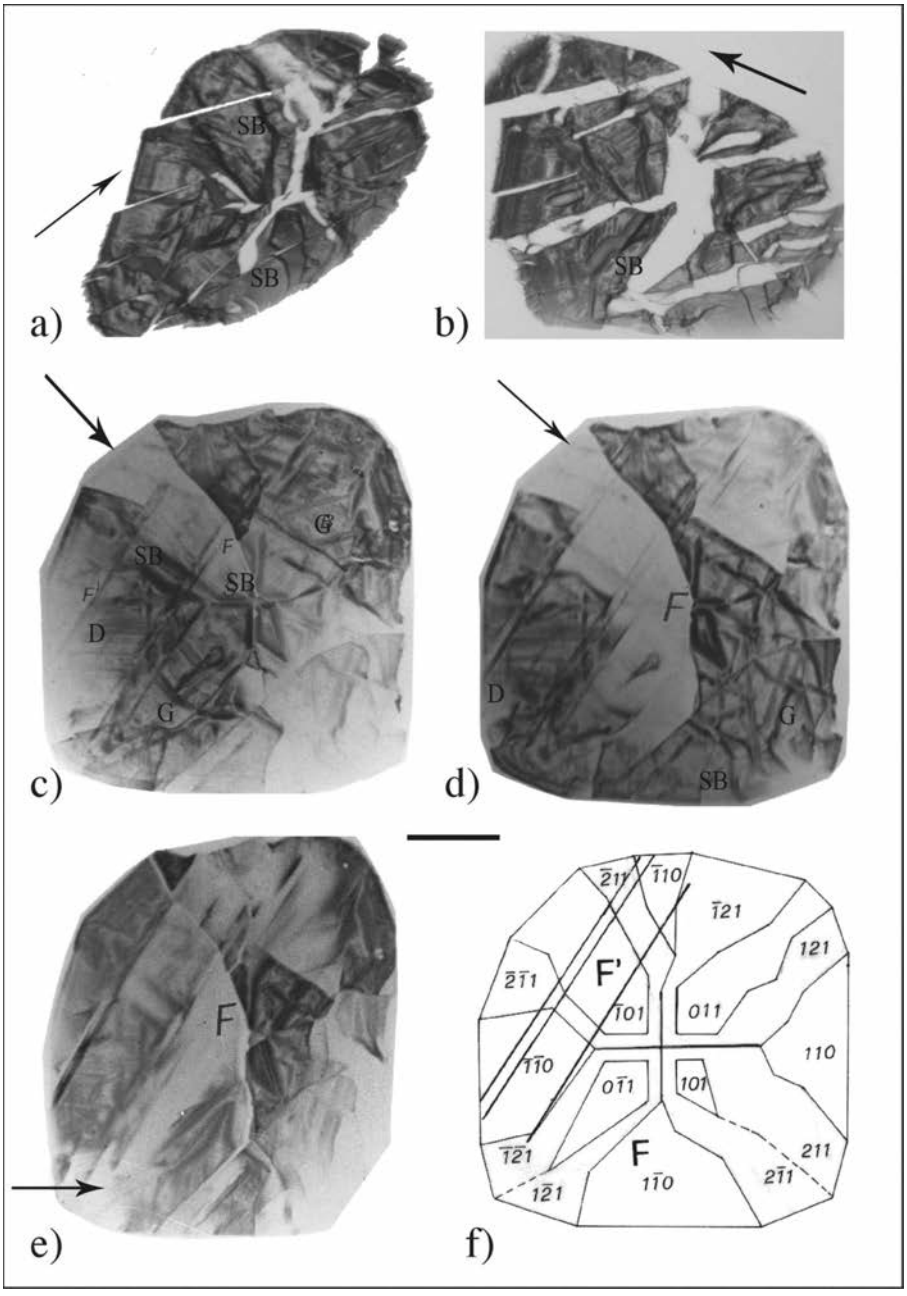

Figure 6. X-ray Topograps of the (001) M3 slice (bar scale = 1 mm). The arrows show the projection of diffraction vectors **g**. G: growth bands; SB: sector boundaries; D: dislocations; F: fractures; F': traces of cleavage. a) SWBXT. **g** = 040. b) SWBXT. **g** = $\bar{4}20$. c) XRDT. **g** = 400. d) XRDT. **g** = 400. e) XRDT. **g** =880. f) schematic drawing of the reconstruction of the growth sector development as obtained by the diffraction contrast analyses.

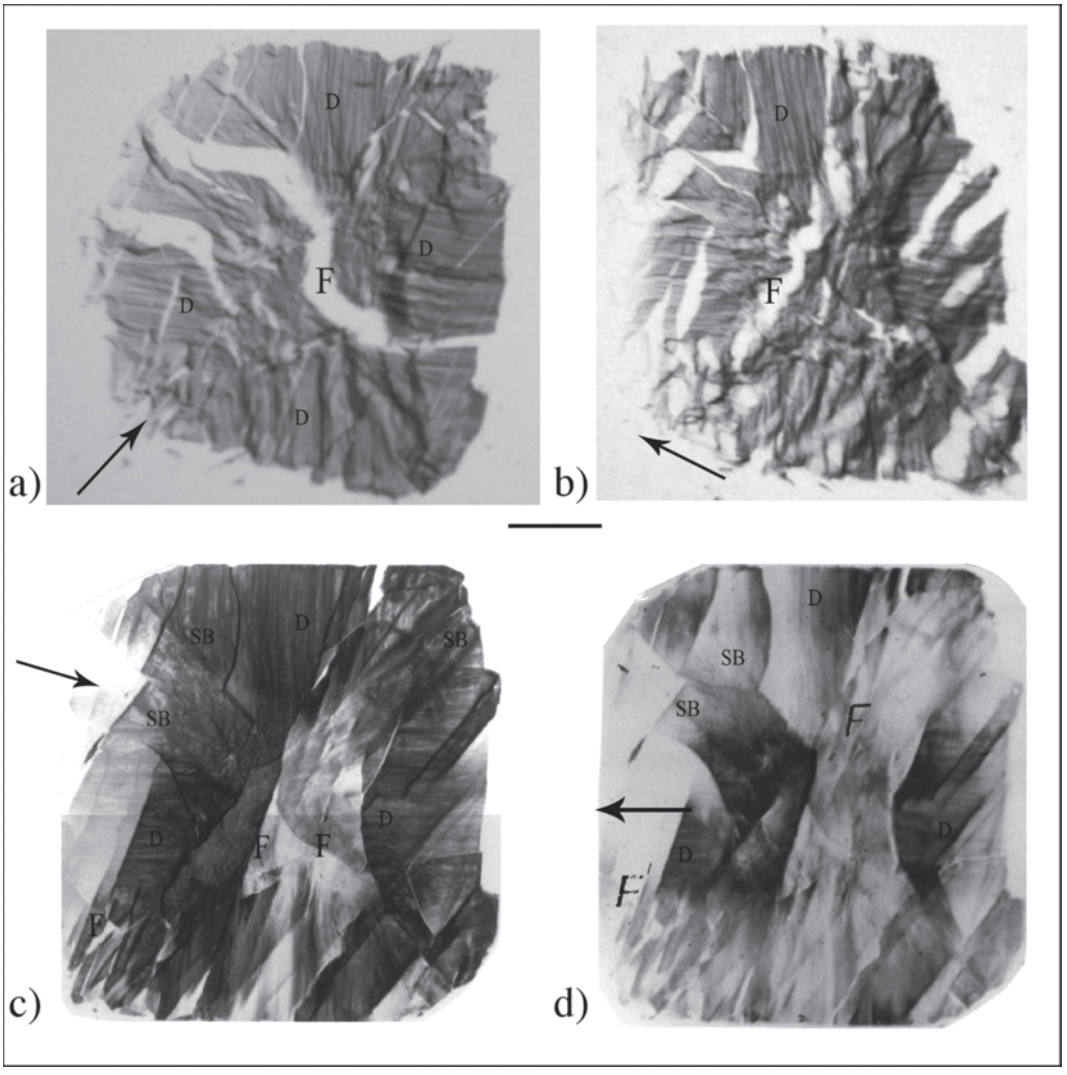

Figure 7. X-ray Topograps of the (001) M4 slice (bar scale = 1 mm). The arrows show the projection of diffraction vectors **g**. D: dislocations; SB: sector boundary; F fracture; F': trace of (110) cleavage. a) SWBXT. **g** = 040. b) SWBXT. **g** = $\bar{4}$00. c) XRDT. **g** = 420. d) XRDT. **g** = $\bar{8}\bar{8}$0.

the theoretical schematic drawings shown in Figures 1d and 1e.

In all the topographs, dislocation bundles D can be observed, even if in each slice their density is different. Most of them present an individual contrast which is generally not resolved due to their high density. However, it can be observed that they are generally nucleated from inclusions I absorbed during growth either at SB (Figure 5a) or at G.

In the topographs of the MG and M3 slice, the *d*{110} growth sectors show a higher density of

dislocation bundles while in the *n*{211} growth sectors only growth bands can be observed (Figures 4a, b, c; Figures 6c, d, e). Instead, in the topographs of the M4 slices, a high density of dislocation bundles characterises all the growth sectors and complicates the identification of other defects (Figure 6).

The characterisation of dislocations using the extinction criterion showed that the most of the dislocations are in fact edge dislocations. For example, in the MG slice, the dislocations of ($\bar{1}$10) growth sectors observed with **g**=004 (Figure 5a) are out of contrast with diffraction vector **g** = $\bar{8}$80 and **g** = 3$\bar{2}$0 (Figures 5b, c). These extinctions of contrasts indicate that in the both cases the condition $|\mathbf{g} \cdot \mathbf{b}| = 0$ is satisfied and, therefore, the Burger vector **b** belongs to the ($\bar{1}$10) plane with direction [001]. Since the unit vector parallel to dislocation line **l** belongs to the [$\bar{1}$10] directions, it can be concluded that $\mathbf{l} \perp \mathbf{b}$ and, therefore, that the dislocations are characterized by a strong edge component. Dislocations D with a strong edge component are also characterised on slice M3, where the dislocations of growth sector ($\bar{1}\bar{1}$0) observed with **g** = 400 (Figures 6a, b, c and d) are out of contrast with diffraction vector **g** = $\bar{8}\bar{8}$0 (Figure 6e). The M3 slice shows a lower dislocation density with respect to the other samples. However, the analyses of the diffraction contrasts of this slice enable the reconstruction of an outstanding development of growth sectors (Figure 6f).

EPMA

All the slices were investigated through Electron Microprobe Analysis (EPMA). The orientation of traverse microanalyses was chosen in order to cross the different growth stages and the different growth sectors. The most important results show concentration variations of mainly TiO_2 and, subordinately, the other oxides investigated (SiO_2, Al_2O_3, FeO_{tot}, MgO, MnO and CaO). In fact, in all the samples, TiO_2 decreased from core to rim crossing the different growth stages. As can be observed in Figure 7, the decline of this oxide between the core and the rim reached almost 50% in some cases.

In most of the examined slices, an increase of SiO_2 from core to rim can be seen. Unfortunately, the entity of the chemical concentration variations of the other oxides often fell into the error bar and thus was below the detection limit of a microprobe. However, considering the chemical analyses carried out on the GRT slice having a stronger colour zoning in its *n* growth sectors (Figure 1b), these variations assume a greater meaning. Additionally, Figure 7 illustrates the chemical profiles related to the orientation of traverse microanalyses on the GRT slice. The main chemical concentration variations are recorded crossing the different growth stages and primarily concern the decreasing amount of TiO_2 from core to rim while those of SiO_2 increase. Beyond these main concentration variations, lower variations also occurred crossing the different growth sectors. In particular, a small but meaningful enrichment of TiO_2 and a decrease of Al_2O_3 take place in correspondence with the *n* growth sectors confirming that sector zoning also occurs (Figure 7).

Discussion and Conclusions

Growth defects and growth mechanism

Growth bands, sector boundaries, dislocations and zonings represent the main defects found in pyroclastic titanian andradite crystals from Colli Albani. The analysis of X-ray topographic contrasts leads to the conclusion that these defects were formed during growth whereas the fractures most likely formed in the post-growth phase. Growth bands G, observed in the M3 and MG slices, record variations of growth conditions. In fact, their topographic contrasts depend on periodic incorporation of impurities or non-stoichiometric material due to variations in microscopic growth rate or diffusion layer

thickness which can be induced by convection instabilities related to temperature fluctuations. They appear only in the sectors in which incorporation of impurities and non-stoichiometric material are associated with a very small relative variation of the lattice constants between adjacent striations (Authier, 1977; Robert et al., 1981).

The extinction of growth bands G observed in Figure 5b indicates that the contrast observed depend upon displacements normal to the $(\bar{1}10)$ growing faces. Since growth bands were observed only in samples M3 and MG, due to the high density of dislocation bundles in the topographs of M4, it could be concluded that samples M3 and MG grew under conditions of lower temperature fluctuations and cooling rates with respect those of sample M4.

Such a hypothesis is also supported by the higher absorption of primary melt inclusions which was observed in the M4 slices. In fact, melt inclusion absorption, generally, depends on a quite high growth rate that is common in high temperature solution growth (volcanic environment). However, the devitrification of glass and the crystallization in daughter minerals indicates a relatively slow cooling.

Sector boundary contrasts SB, observed in samples MG and M3 (Figures 4, 5 and 6) were visible when neighbouring growth sectors either had a difference in their lattice constants of about $3 \cdot 10^{-5}$ Å because of a different impurity content, or were misoriented by about 3" with respect to each other (Authier, 1977a, b; Robert et al., 1981). Such defects can show the shape and the space-time development of growth sectors.

In all the studied slices, the dislocations appear to be nucleated from solid inclusions and appear to be generally associated in high thick bundles. When the high density of defects and fractures did not inhibit our ability to determine the Burgers vector, dislocations with a strong edge component were found. Since the orientation of dislocation bundles are generally perpendicular to the growing faces to minimise their elastic energy (Klapper, 1972), their resolution with the SB and G diffraction contrasts can contribute to the reconstruction the morphological evolution vs. time of the slices. Such reconstruction shows that the morphology of crystals was faceted from growth onset and that the most important faces were {110} and {211}. Moreover, the different development of these forms suggests different growth rates: the predominant {110} faces may have grown more slowly than the {211}. These results confirm previous theoretical studies on the morphology of garnets (Bennema et al., 1983; Boutz and Woensdregt, 1993). In addition, the irregular shape of growth sectors, as determined by the SB diffraction contrasts, indicates significant fluctuations in the aforementioned growth rates during crystallisation. On the other hand, the capture of foreign material on the different surfaces of a growing crystal, as shown by G defects, is clearly favoured by increasing roughness on the surface and thus an increasing growth rate. Nevertheless, it is worth pointing out that roughness depends on the density of step sites which are the only places where the growth units can attach onto the flat growing surfaces.

The well developed and faceted morphology of garnets studied in this paper indicates that the growth mechanism probably occurred by "layer by layer" and not through continuous growth. There are two layer-spreading growth mechanisms: two-dimensional nucleation and spiral growth. The latter is related to the "self perpetuating" of screw dislocations and promotes crystal growth at lower supersaturation. In our samples, we only found dislocations with strong edge components and thus the spiral growth mechanism could be excluded. Consequently, it can be hypothesized that the Ti-rich andradites from Colli Albani underwent a layer-spreading growth mechanism by two-dimensional nucleation.

Chemical zoning

The reconstruction of morphology was particularly useful in distinguishing two different

types of zoning. In fact, the mutual relation between chemical profiles and the arrangement of growth sectors made it possible to localise the chemical concentration variations of SiO_2, TiO_2 and Al_2O_3 in correspondence with growth stage boundaries and/or growth sectors (*n* and *d* in Figure 7). The major elements are concentrically zoned about the garnet core in the classic bell-shaped profiles: the main chemical concentration variations affect successive growth stages and thus can be considered indicative of growth zoning. Moreover, the increase of TiO_2 and decrease of Al_2O_3, observed crossing the *n*{211} growth sectors, can be classified as sector zoning and are responsible for the previous optically observed colour zoning.

The two types of chemical zonings and their genetic meaning are very different and this disparity may be responsible for the erroneous petrogenetic information. Concentric zoning consists of compositional variations simultaneously affecting all growing faces, irrespective of their crystallographic orientations (Smith and Lofgren, 1983; Spry, 1987). In fact, this type of zoning will record the evolution of the physio-chemical conditions occurring in the growth environment during the crystallisation process. On the contrary, sector zoning consists of compositional variations between individual growth sectors not related by symmetry. It occurs in physio-chemical conditions that may be constant and uniform. Its origin is due to the selective absorption of minor elements by time equivalent portions of different growth sectors. Such absorption can only arise during the growth process and may depend either upon different growth rates of crystal faces and/or structural factors (Dowty, 1976; Nakamura, 1973; Leung, 1974; Larsen, 1981; Reeder and Prosky, 1986; Shearer and Larsen, 1994).

As is the case here, the different genetic meaning of concentric and sector zoning should be further confirmed by different substitution mechanisms. Taking into account the general formula of garnet $X_3Y_2(ZO)_4$, the concentration variations observed crossing successive growth stages of TiO_2 compared with SiO_2 variations, seem to be due mainly to $Si^{4+} \leftrightarrow Ti^{4+}$ substitution at the Z site (concentric zoning); whereas the TiO_2 and Al_2O_3 variations, observed in correspondence with *n*{211} growth sectors could be due to the atomic replacement $Al \leftrightarrow Ti^{4+}$ at the Y site (sector zoning). The charge balance may be guaranteed by a concurrent substitution of a bivalent cation M^{2+} with Ti^{4+} in place of the Al. These hypotheses can be confirmed only with a complete crystal chemical characterization of these garnets which could reveal the exact distribution over different crystallographic sites of Al, Fe and Ti and the valence states of the coexisting transition elements (Fe and Ti). However, the substitution mechanisms hypothesized in this study are confirmed by those proposed in a previous study carried out on a Ti-rich andradite sample coming from the same site at Colli Albani and having similar chemical composition and chemical zonings as those found in this study (Agrosì et al., 2002). In this previous work, two crystal fragments extracted respectively from the *d*{110} and *n*{211} growth sectors were investigated using EPMA, Single Crystal X-ray Diffraction and Mössbauer Spectroscopy. Two substitution mechanisms were found in the (110) fragment:

morimotoite substitution:

$M^{2+}(Y)+M^{4+}(Y) \leftrightarrow 2M^{3+}(Y)$ M^{2+}= Mg, Mn^{2+}
M^{3+}= Al, Fe^{3+}
M^{4+}= Ti, Zr

schorlomitic substitution:

$Ti^{4+}(Y)+Fe^{3+}(Z) \leftrightarrow Si^{4+}(Z)+Al^{3+}(Y)$

whereas only a single heterovalent schorlomitic substitution mechanism was determined in the (211) fragment.

Hence, it can be deduced quite accurately that the sector zoning is due to an atomic replacement of $Al \leftrightarrow Ti^{4+}$ at the Y site, even if the true substitution mechanism, according to the aforementioned schorlomitic substitution, regards the Z site as well. Instead, the concurrent

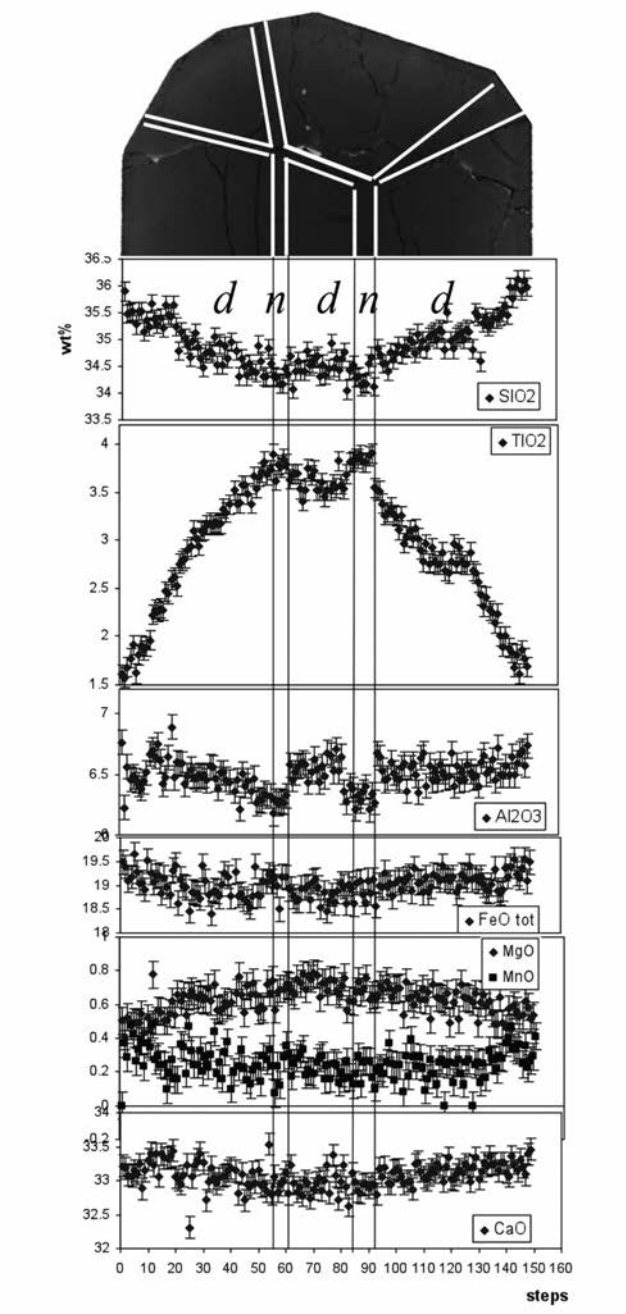

Figure 8. Slice GRT. Microanalyses performed along the traverse shown in the micrograph. The sector boundaries of the *n* growth sectors are highlighted in white. The step is 50 μm. Vertical lines indicate boundaries between *d* and *n* growth sectors. The error bars are ± 1 standard deviation, as calculated from counting statistics.

substitution mechanisms (morimotoitic and schorlomitic substitution) found in the *d* growth sector reveal that the concentric zoning is due partially to $Si^{4+} \leftrightarrow Ti^{4+}$ substitution and that this substitution only appears to occur at the Z site.

Growth Marks

Primary melt inclusion absorption and concentric zoning represent common features in crystals grown during magmatic crystallisation (Jambon, 1996). Most likely, the zoning occurring above the different growth stages reflects the physio-chemical evolution of the growth environment. Moreover, the absorption of rod-like melt inclusions and the incorporation of impurities and non-stoichiometric materials at the sector boundaries (SB) and in correspondence of growth stage boundaries (G) may arise because of a change in crystallization conditions. Therefore, it can be deduced that melt inclusions, growth bands, sector boundaries and concentric zoning should be considered as growth marks characterizing the Ti-rich andradite crystals studied. This is due to the fact that they represent distinctive features of their growth environment. However, edge dislocations and sector zoning may be classified also as growth marks because they provide further noteworthy information about the crystallization condition of these samples. In fact, the reconstruction of the morphological evolution of the Ti-rich andraditic garnets carried out using structural defect analyses and the characterisation of only dislocations with strong edge component suggest that the minerals under investigation grew through a layer - spreading growth mechanism by two-dimensional nucleation.

Previous studies on synthetic and natural garnets grown under hydrothermal conditions have demonstrated that all examined crystals exhibited {110} and {211} faces with polygonal spirals on {110} and growth steps on {211} (Jamtveit and Andersen, 1992; Milke, 2004). The occurrence of round growth spirals on {211}faces were also found in some synthetic hydrothermal garnets (Milke, 2004). Conversely, minerals grown under cooling from high magmatic temperatures, at high supersaturation, present generally rough growing faces and fast continuous growth. As supersaturation decreases, the growth mechanism turns into layer growth by two-dimensional nucleation or at even lower supersaturation and lower temperature (most likely hydrothermal conditions) into spiral growth by screw dislocations (Sunagawa, 2005). Therefore, it can be concluded that the presence of edge dislocations to the absence of screw dislocation characterisation and the consequent determination of layer-spreading growth by two-dimensional nucleation represent a further distinctive growth mark for the Ti-rich andradite from Colli Albani. In fact, such a mechanism distinguishes the growth environment of these garnets from the hydrothermal and metasomatic environment in which the spiral growth mechanism generally occur (Sun and Baronnet, 1989; Agrosì et al., 2006) and thus characterises it.

Furthermore, some considerations can be made regarding the colour zoning and sector zoning described on the GRT slice. The chemical differences between non-equivalent growth sectors characterise a sample in which the predominant development of *d*{110} on *n*{211} forms arises. This implies that the *n*{211} growth sectors grew more rapidly than the other sectors by the "layer by layer" mechanism. Therefore, the lattice strain effect, caused by the schorlomitic substitutions, seems to be particularly connected to the higher growth rate of the {211} sectors; which in turn, is directly proportional to the attachment energy (Hartmann and Bennema, 1980). Lastly, the "multiphasic" character of primary melt inclusions containing generally silicate glass or its devitrified equivalent plus a shrinkage/vapour bubble and, in some cases, also several daughter crystals indicates a quite slow cooling. Therefore, it can be concluded that the growth marks found in this study represent

distinctive defects that characterise the Ti-rich andradites from Colli Albani and distinguish them from others grown in different conditions. In addition, these growth marks indicate that the crystallisation of these minerals occurred under slow cooling. This fact confirms data in the literature indicating that the growth of garnets at Colli Albani may have resulted from a slow and deep crystallization of leucite melt (Fornaseri et al., 1963).

Acknowledgements

The authors are very grateful to Prof. Sergio Lucchesi, who is remembered with great affection, for his suggestions about the study of the sector zoning and the application of the growth mark concept made in this work. Moreover, the authors thank Mr. Marcello Serracino (Centro Studio per il Quaternario e l' Evoluzione Ambientale of CNR, Rome, Italy) for the Electron Microprobe measurements and Mr. Pasquale Trotti (Dipartimento Geomineralogico-University of Bari) for the photographs. The authors are grateful to dr. Carlaina Brown, who revised the English text. The research was funded by MURST grants to E. S.

References

Agrosì G., Schingaro E., Pedrazzi G., Scandale E. and Scordari F. (2002) - A crystal chemical insight into sector zoning of a titanian andradite (melanite) crystal. *European Journal of Mineralogy*, 14, 785-794.

Agrosì G., Bosi F., Lucchesi S., Melchiorre G. and Scandale E. (2006) - Mn-tormaline crystals from island of Elba (Italy): Growth history and growth marks. *American Mineralogist*, 91, 944-952.

Agrosì G., Lattanzi P., Ruggieri G. and Scandale E. (1992) - Growth history of a quartz crystal from growth marks and fluid inclusions data, *Neues Jahrbuch für Mineralogie*, Mh, 7, 289-294.

Agrosì G., Scandale E. and Digennaro M.A. (2001) - Growth defects of a melanite crystal. *Neues Jahrbuch für Mineralogie*, Mh, 176, 89-107.

Authier A. (1977) - X-ray and Neutron Topography of Solution-grown Crystals. -In: *Current topics in Materials Science*. (eds): E. Kaldis and J.H. Scheel (North-Holland, Amsterdam), 2, 515-520.

Bennema P., Giess E.A. and Weidenborner J.E. (1983) - Morphology of garnets and structure of F slices determined from PBC analysis. *Journal of Crystal Growth*, 62, 41-60.

Bosi F., Agrosì G., Lucchesi S., Melchiorre G. and Scandale E. (2005) - Mn-tourmaline from island of Elba (Italy): *Crystal chemistry. American Mineralogist*, 90, 1661-1668.

Boutz M.M.R. and Woensdregt C.F. (1993) - Theoretical growth forms of natural garnets. *Journal of Crystal Growth*, 134, 325-336.

Downes M.J. (1974) - Sector and oscillatory zoning in calcicaugites from M. Etna, Sicily. *Contributions to Mineralogy and Petrology*, 47, 187-196.

Dowty E. (1976) - Crystal structure and crystal growth: II. Sector zoning in minerals. *American Mineralogy*, 61, 460-469.

Fornaseri M., Scherillo A., Ventriglia U. (1963) - La regione vulcanica dei Colli Albani -Vulcano Laziale - Consiglio Nazionale delle Ricerche, Aziende Tip. Eredi dott. Bardi, Roma, 407.

Graziani G., Lucchesi S. and Scandale E. (1990) - General and specific growth marks in pegmatite beryls. *Physics and Chemistry of Minerals*, 17, 379-384.

Graziani G., Lucchesi S., Scandale E. (1990) - General and specific growth marks. *Physics and Chemistry of Minerals*, 17, 379-384

Hartmann P. and Bennema P. (1980) -The attachment energy as habit controlling factor. *Journal of Crystal Growth*, 49, 145-156.

Huang X.R. LauePt program, version 2.1 Stony Brook Copyleft 1998-2003.

Jambon A. (1996) - Melt growth. -In: Crystal Growth in Earth Sciences. (eds): E. Scandale and A. Baronnet, EDISU, Torino (Italy), 98-128.

Jamtveit B. and Andersen T.B. (1992) - Morphological instabilities during rapid growth of metamorphic garnets. *Physics and Chemistry of Minerals*, 19, 176-184.

Klapper H. (1972) - Elastiche Energie und Vorzugstructungen geradlinger Versetzungen in aus der Lösung gewachsenen organischen Kristallen., *Physica Status Solidi*, A14, 99-106.

Lang A.R. (1959) - The projection topograph: a new method in X-ray diffraction microradiography. *Acta Crystallographica*, 12, 249-250.

Larsen L.M. (1981) - Sector zoned aegirinae from Illìmaussaq alkaline intrusion, South Greenland.

Contributions to Mineralogy and Petrology, 76, 285-291.

Leung I.S. (1974) - Sector-zoned titanaugites: morphology, crystal chemistry, and growth. *American Mineralogist*, 59, 127-138.

Milke R. (2004) - Spiral growth of grossular under hydrothermal conditions. *American Mineralogist*, 89, 211-218.

Nakamura Y. (1973) - Origin of sector zoning of igneous clinopyroxenes. *American Mineralogist*, 58, 986-990.

Reeder R.J. and Prosky J.L. (1986) - Compositional sector zoning in dolomite. *Journal of Sedimentary Petrology*, 56, 237-247.

Robert M.C., Lefaucheux F. and Sauvage M. (1981) - Quantitative lattice parameter mapping in $Sr(NO_3)_2$ and $Ba(NO_3)_2$ crystals. *Journal of Crystal Growth*, 52, 976-982.

Scandale E., Lucchesi S. and Graziani G. (1990) - Growth defects and growth marks in pegmatite beryls. *European Journal of Mineralogy*, 2, 305-311.

Scandale E., Stasi F. and Zarka A. (1983) - Growth defects in a Quartz Druses. ac dislocations. *Journal of Applied Crystallography*, 16, 399-403.

Scandale S.and Stasi F. (1985) - Growth defects in quartz druses. a-Pseudo-basal dislocations. *Journal of Applied Crystallography*, 18, 275-278.

Shearer C.K. and Larsen L.M. (1994) - Sector-zoned aegirine from Illìmaussaq alkaline intrusion, South Greenland: Implications for trace-element behaviour in pyroxene. *American Mineralogist*, 79, 340-352.

Smith R.K. and Lofgren G.E. (1983) - An analytical study and experimental study of zoning in plagioclase. *Lithos*, 16, 153-168.

Spry P.G. (1987) - Compositional zoning in zincian spinel. *Canadian Mineralogist*, 25, 97-104.

Sun B.N. and Baronnet A. (1989) - Hydrothermal growth of OH-phlogopite single crystals. I Undoped growth medium. *Journal of Crystal Growth*, 96, 265-276.

Sunagawa I. (2005) - Crystals: Growth, Morphology and Perfection. Cambridge University press (and references therein).

Submitted, October 2010 - Accepted, January 2011